Experimental Identification of Electric Field Excitation Mechanisms in a Structural Transition of Tokamak Plasmas

メタデータ	言語: eng
	出版者:
	公開日: 2021-06-28
	キーワード (Ja):
	キーワード (En):
	作成者: Kobayashi, T., Itoh, K., Kamiya, K., Miura, Y., Nagashima, Y., Fujiwara, A., Inagaki, S., Ida, K., Hoshino, K.
	メールアドレス:
	所属:
URL	http://hdl.handle.net/10655/00012522

SCIENTIFIC REPORTS

Experimental Identification of Electric Field Excitation Mechanisms in a Structural Transition of Tokamak Plasmas

T. Kobayashi[1], K. Itoh[1,2], T. Ido[1], K. Kamiya[3], S.-I. Itoh[2,4], Y. Miura[5], Y. Nagashima[2,4], A. Fujisawa[2,4], S. Inagaki[2,4], K. Ida[1,2] & K. Hoshino[3]

Self-regulation between structure and turbulence, which is a fundamental process in the complex system, has been widely regarded as one of the central issues in modern physics. A typical example of that in magnetically confined plasmas is the Low confinement mode to High confinement mode (L-H) transition, which is intensely studied for more than thirty years since it provides a confinement improvement necessary for the realization of the fusion reactor. An essential issue in the L-H transition physics is the mechanism of the abrupt "radial" electric field generation in toroidal plasmas. To date, several models for the L-H transition have been proposed but the systematic experimental validation is still challenging. Here we report the systematic and quantitative model validations of the radial electric field excitation mechanism for the first time, using a data set of the turbulence and the radial electric field having a high spatiotemporal resolution. Examining time derivative of Poisson's equation, the sum of the loss-cone loss current and the neoclassical bulk viscosity current is found to behave as the experimentally observed radial current that excites the radial electric field within a few factors of magnitude.

Self-organization in the structure-turbulence system has been widely recognized as one of the central issues in modern physics. An abrupt reduction of the turbulent transport in toroidal plasmas, i.e., the L-H transition[1], is the prototypical example of the turbulence structure formation in high temperature plasmas, and has been intensively studied. In recent decades, much progress has been achieved in understanding of the physical mechanism, such as proposal of theoretical models for the electric field bifurcation[2–4] and the turbulence suppression[5,6], experimental confirmation of the radial electric field[7–9], and others. Time derivative of Poisson's equation is examined to elucidate responsible physics of the electric field bifurcation[10], and has been applied to the plasmas in the Compact Helical System[11]. Electrode biasing experiment[12] has provided a way to understand the electric field bifurcation and the structure formation[13–15]. Consecutive emergence and decay of the transport barrier just before the L-H transition, the so-called limit-cycle oscillation (LCO), are known to occur spontaneously, above which the physics of the H-mode has been discussed intensively (see refs 11,16–18 and references therein). The important role of the enhancement of the toroidal dielectric constant[10] has been known[19], including an experimental confirmation of the toroidal return flow[20,21]. Today, the quantitative validation of physical processes that include the toroidal effects of the dielectric constant can be investigated.

Here we perform systematic and quantitative validation study for the key physics for the radial electric field excitation in the L-H transition. The experiments were conducted in the JFT-2M tokamak. Heavy Ion Beam Probe (HIBP) measurement was performed for direct observations of the radial electric field, the density gradient length, and the turbulent electrostatic potential fluctuation with a high spatiotemporal resolution. Taking into account the toroidal effect on the dielectric constant, we found that the sum of the loss-cone loss current and the neoclassical bulk viscosity current[10] meets the experimentally observed current that excites the radial electric field

[1]National Institute for Fusion Science, Toki 509-5292, Japan. [2]Research Center for Plasma Turbulence, Kyushu University, Kasuga 816-8580, Japan. [3]National Institutes for Quantum and Radiological Science and Technology, Naka 311-0193, Japan. [4]Research Institute for Applied Mechanics, Kyushu University, Kasuga 816-8580, Japan. [5]Japan Atomic Energy Agency, Tokai 319-1184, Japan. Correspondence and requests for materials should be addressed to T.K. (email: kobayashi.tatsuya@LHD.nifs.ac.jp)
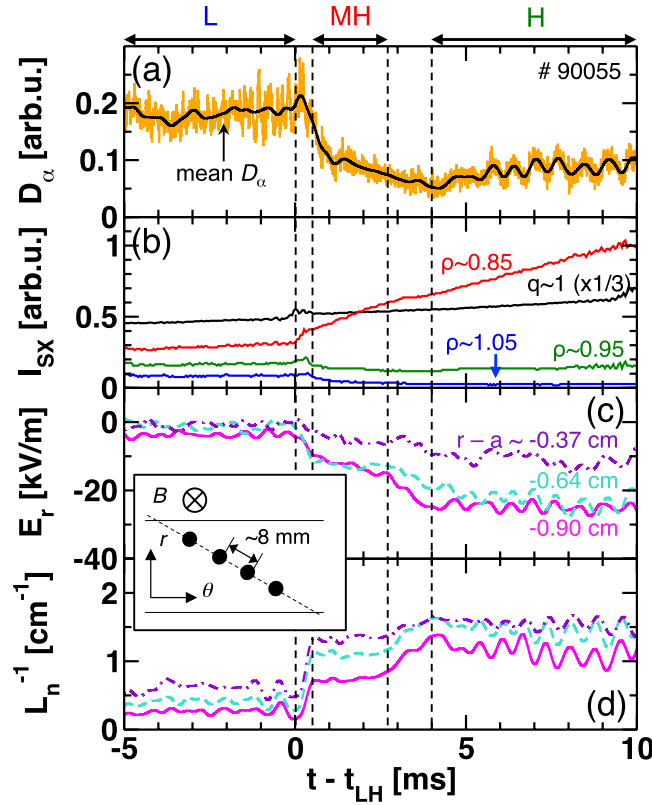
Figure 1. Time traces of (**a**) D_α emission, (**b**) soft-x-ray emission intensity I_{SX}, (**c**) radial electric field E_r, and (**d**) inverse density gradient length L_n^{-1} at $r - a \sim -0.6 \pm 0.3$ cm. Radial position of E_r and L_n^{-1} signals are labeled in Fig. 1(c) in color. The insert shows a schematic view of the measurement configuration, where two horizontal lines and four circles show the magnetic surfaces and the center of HIBP measurement positions, respectively.

during the L-H transition. A small contribution of the turbulent Reynolds stress was also confirmed. This is the first experimental study that quantitatively and systematically validates the theoretical models of the electric field bifurcation in the L-H transition.

Results

Experimental setup.   It is known that the L-H transition occurs with a heating power above a threshold. The experiments were conducted with the marginal condition (slightly above the threshold heating power) for the L-H transition. See "Methods" for more details of the plasma parameters. Multipoint measurement of the electrostatic potential ϕ and the electron density n_e is performed with a heavy ion beam probe (HIBP). In the series of experiments, the radial positions of the HIBP sample volumes were scanned in the edge region(-5 cm $< r - a < 0$ cm, where $r - a$ is the radial distance from the saparatrix), in a shot-to-shot basis. The two key parameters of the study, the radial electric field $E_r \equiv -\partial\phi/\partial r$ and the inverse density gradient length $L_n^{-1} \equiv -n_e^{-1}\partial n_e/\partial r$, are evaluated by taking the difference of two HIBP signals measured at neighboring sample volumes. The advantage of the HIBP measurement is that one can directly obtain the radial electric field even during the transition, unlike some indirect methods that employ the radial force balance equation.

L-H transition in the discharge.   Figure 1 shows the typical time evolution of (a) the edge D_α emission, (b) the soft-x-ray emission intensity I_{SX}, (c) mean value of the radial electric field E_r, and (d) mean value of the inverse density gradient length L_n^{-1} at a discharge (shot number #90055). The insert shows a schematic view of the measurement configuration. The measurement position is $r - a \sim -0.6 \pm 0.3$ cm, where the bottom of the electric field well appears in the H-mode [see Fig. 2(a) for the E_r profile.]. Here the poloidal direction θ is taken in the electron-diamagnetic drift direction following the right-hand rule (r, θ, z), where the toroidal magnetic field direction is taken as z direction. Mean component of the parameters is calculated by use of a digital low-pass filter with a cut-off frequency of 2 kHz, to filter out the LCO ($f \sim 4.5$ kHz) or other dynamics having higher frequencies. The discharge shows the two-step transition[22]. The onset time of the first transition is generally defined as the moment when the negative electric field starts to evolve (potential to decrease) at the position of the transport barrier. This is well correlated to the moment when the heat pulse of the sawtooth crash reaches the edge $\rho \sim 0.95$ and the edge D_α emission drops. We call the moment t_{LH}, which can be defined through I_{SX}. After a short stagnation at a meta-stable state for ~ 2 ms, which we call the meta-H (MH) mode, the second transition occurs. The time scale of the first growth of the radial electric field (L-MH transition) [$O(100\,\mu s)$] is much faster than that of
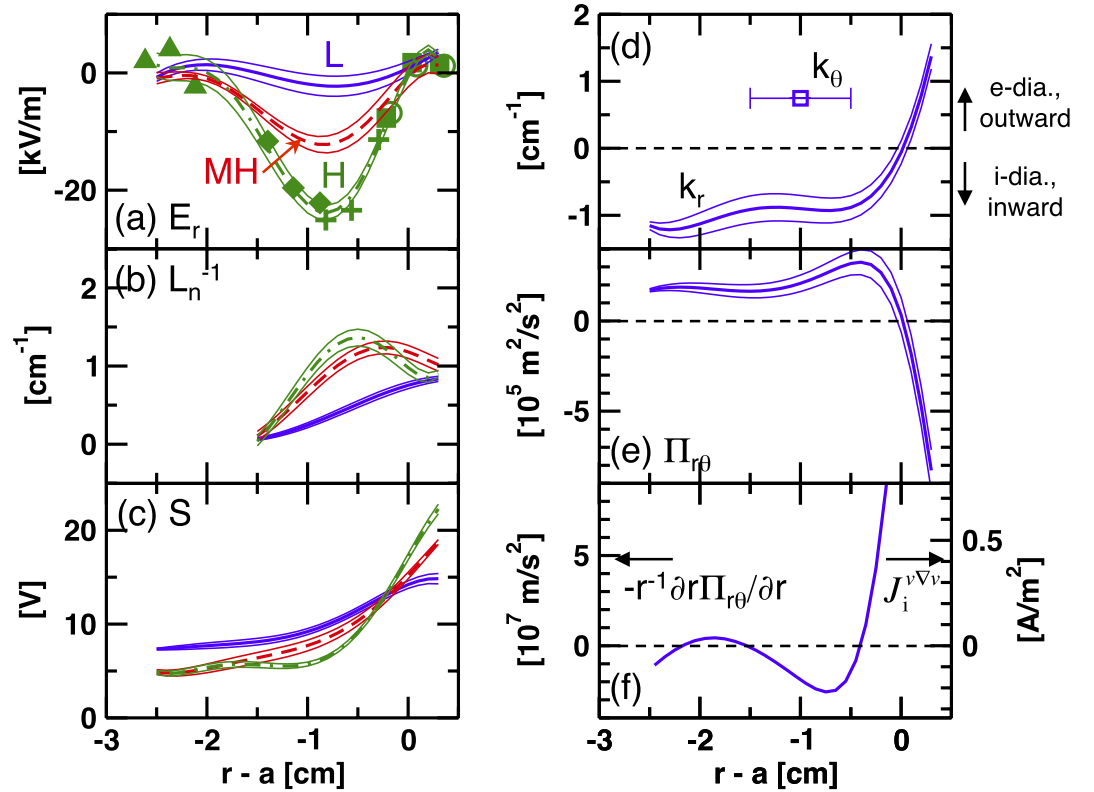
Figure 2. Mean radial profiles of (**a**) radial electric field E_r, (**b**) inverse density gradient length L_n^{-1}, (**c**) turbulence amplitude S, (**d**) radial and poloidal turbulence wavenumbers k_r (curves) and k_θ (open squares), respectively, (**e**) turbulent Reynolds stress $\Pi_{r\theta}$, and (**f**) negative divergence of turbulent Reynolds stress $-r^{-1}\partial r\Pi_{r\theta}/\partial r$.

the second growth (MH-H transition) [O(1 ms)]. Time trace of the soft-x-ray signal shows that the sawtooth crash and/or coinciding events might trigger the L-MH transition.

Mean profiles of the radial electric field E_r and the inverse density gradient length L_n^{-1} are shown in Fig. 2(a,b). Due to the restriction of the measurement volume locations, the inverse density gradient length can be computed only in the very edge region. Looking at the time evolution of the D_α signal in detail, five discharges with a high reproducibility and different HIBP measurement positions are selected for the use of the profile evaluation[23]. Time average is taken for each confinement state, as $-5\,\text{ms} \le t - t_{\text{LH}} \le 0\,\text{ms}$ (L-mode), $1\,\text{ms} \le t - t_{\text{LH}} \le 2\,\text{ms}$ (MH-mode), and $6\,\text{ms} \le t - t_{\text{LH}} \le 10\,\text{ms}$ (H-mode). In Fig. 2(a), five kinds of symbols are plotted, showing the mean values from different discharges. A fifth-degree polynomial fits the points, where the fitting error are evaluated from the scatter of the points from the fitted curve. Through the two steps of transitions, the electric field well and its shear grow gradually. At the L-MH transition, the edge density pedestal is mostly completed, then the peak position is slightly shifted inward after the MH-H transition. The radial profile of the turbulence amplitude S is shown in Fig. 2(c), where it is defined as the potential fluctuation having a frequency range of $30\,\text{kHz} \le f \le 90\,\text{kHz}$. The turbulence amplitude is suppressed step by step in $r - a \le -0.3\,\text{cm}$. Meanwhile, it seems to grow at the outer radii. Turbulence wavenumber can also be investigated from the phase difference of the HIBP signals in the L-mode. Figure 2(d) shows the radial wavenumber k_r and the poloidal wave number k_θ in the L-mode. The horizontal error bar in the open square shows an uncertainty of the measurement position for the k_θ determination. Considering the Doppler shift by a small $E \times B$ velocity in the L-mode, the turbulence is found to propagate in the electron-diamagnetic drift direction in both the laboratory frame and the plasma frame. The density and potential turbulent fluctuations have almost the same relative amplitudes, a high cross coherence, and the phase difference of $(0.1 - 0.2) \times 2\pi$ (drift waves linearly unstable)[18]. Therefore, the instability is categorized to drift waves.

Model validation. Bifurcation of the radial electric field is discussed through examining the ambipolar condition of the radial current[2,3]. We start from time derivative of Poisson's equation

$$\varepsilon_\perp \varepsilon_0 \frac{\partial E_r}{\partial t} = -J_r,$$

(1)

where $\varepsilon_\perp$ is the relative dielectric constant of toroidal plasmas[10,19]. It is given as

$$\varepsilon_\perp = 1 + M_{\text{tor}} \frac{c^2}{v_A^2},$$

(2)

where c/v_A denotes the ratio between the speed of light and the Alfvén velocity ($v_A = B/\sqrt{n_i m_i \mu_0}$). Inertia enhancement factor in the banana regime is given as

$$M_{\text{tor}} \sim 1 + \frac{1.6q^2}{\sqrt{\varepsilon_t}} \sim 30,$$

(3)

where q is the safety factor and $\varepsilon_t = a/R$ is the inverse aspect ratio. In the toroidal devices, the inertia enhancement factor takes a larger value than unity. Since the $E \times B$ velocity in the poloidal direction has a finite divergence due to the toroidal geometry, the return flow that maintains the divergence free condition is generated in the direction of the magnetic field line. As a result, effective acceleration in the poloidal direction is reduced by the factor M_{for}[10,19]. The toroidal return flow is experientially observed in ASDEX-U[20] and JT-60U[21].

The model of the radial current is given as

$$J_r = J_i^{\text{lc}} + J_i^{\text{bv}} + J_i^{\nu\nabla\nu} - J_{e-i}^{\text{wave}} + J_i^{\text{CX}} + \text{others},$$

(4)

where the terms in the r.h.s. are contributions of the loss-cone loss, the neoclassical bulk viscosity, the Reynolds stress, the wave convection, and the charge exchange[10]. In ref. 24, quasi-linear part of the wave convection term J_{e-i}^{wave} is related to quasi-linear contribution in the Reynolds stress term $J_i^{\nu\nabla\nu}$ for the case of drift waves. In this discharge, the carbon wall and the carbon divertor seem to make the neutral reflection on the wall relatively weak, which results in a low neutral density in the confinement region[25]. Therefore, we do not take into account J_i^{CX}. The first three terms can be quantitatively examined here at the location of the transport barrier, $r - a \sim -0.6\,\text{cm}$. For the fourth term J_{e-i}^{wave}, only an intuitive model is available[2], which is considered to be important in the L-mode and will be discussed at the later part.

First, the loss-cone loss current J_i^{lc} and the neoclassical bulk viscosity current J_i^{bv} are discussed. These are given as a function of the normalized radial electric field, $X \equiv \rho_p e E_r/T$ ($\rho_p = q\varepsilon_t^{-1}\rho_i$ is the ion gyroradius at the poloidal magnetic field and ρ_i is the ion gyroradius), and the normalized inverse density gradient length, $\lambda \equiv \rho_p L_n^{-1}$, as,

$$J_i^{\text{lc}} = en_e \nu_{ii} \rho_p \frac{\nu_*}{\sqrt{\nu_* + X^4 + (r-a)^4/w_{bi}^4}} \exp\left[-\sqrt{\nu_* + X^4 + (r-a)^4/w_{bi}^4}\right],$$

(5)

and

$$J_i^{\text{bv}} = -en_e D_p \rho_p^{-1}(-\lambda - X) \operatorname{Im} Z(X + i\nu_{ii}/\omega_t),$$

(6)

where $\nu_* = \nu_{ii}/\omega_t \varepsilon^{3/2}$ is the ion collisionality defined as a ratio of the ion-ion collision frequency ν_{ii} and the ion transit angular frequency ω_t, $w_{bi} = q\rho_i/\sqrt{\varepsilon_t} = \sqrt{\varepsilon_t}\rho_p$ is the banana width, and $D_p = \varepsilon_t q\rho_i T/\sqrt{\pi}\, reB$ is a typical diffusivity. Plasma dispersion function $\operatorname{Im} Z(X + i\nu_{ii}/\omega_t)$ is given in ref. 26 as a similar function of Gaussian function $\exp(-X^2)$. The loss-cone loss current J_i^{lc} is caused by the nonambipolar particle flux due to the direct ion loss at the plasma boundary[2]. The neoclassical bulk viscosity current J_i^{bv} includes the *diamagnetic term* in the driving force of the radial electric field[3,13], which is now thought to play a leading role in the L-H transition in high collisionality plasmas[27]. The term λ in the expression of J_i^{bv} [Eq. (6)] indicates the density gradient contribution for the radial electric field excitation. Theoretical prediction of the sum of the two terms $J_i^{\text{lc}} + J_i^{\text{bv}}$ is given in Fig. 3(a), as a function of the normalized radial electric field X and the normalized inverse density gradient length λ. As a first step, we used the plasma parameters such as ν_{ii} and ρ_p in the L-mode for the evaluation of the models although they vary during the transition. The trajectory of the experimental parameters (X, λ) is overplotted. The predicted radial current is the value of the contour on the trajectory. Figure 3(b) shows the experimentally observed radial current density $J_r = -\varepsilon_\perp \varepsilon_0 \partial E_r/\partial t$ [Eq. (1)] and the theoretical prediction $J_i^{\text{lc}} + J_i^{\text{bv}}$ [Eqs (5) and (6)] as a function of the normalized radial electric field. The evaluations of both J_i^{bv} and J_i^{lc} strongly depend on the value of the ion temperature. It is worthwhile to estimate uncertainty of the prediction caused by change of the ion temperature during the transition. Unfortunately, the ion temperature signal with a high time resolution is not available for the discharge. Instead, an edge electron temperature signal obtained from the electron cyclotron emission system, T_e, is used for estimating the time evolution of the ion temperature T_i. The shaded area in Fig. 3(b) is the uncertainty of the prediction. The upper and lower boundaries correspond to the cases $T_i = T_e$ and $\partial T_i/\partial t = 0$, respectively. During the L-MH transition at $X \sim -1$, $J_i^{\text{lc}} + J_i^{\text{bv}}$ is in agreement with the observation within the factor of ~ 2. Contributions from J_i^{bv} and J_i^{lc} seem to be in the same order in the case $\partial T_i/\partial t = 0$ [shown in Fig. 3(b)], meanwhile under the case $T_e = T_i$ the contribution of J_i^{bv} dominates that of J_i^{lc}. After the L-MH transition, J_i^{lc} and J_i^{bv} are reduced due to the large radial electric field. The peak in the $E_r - J_r$ curve at $X \sim -2$ for the MH-H transition is not clear in these terms, since the established models do not focus on multi-step transitions. Moreover, in the L-mode, a finite positive offset of the radial current $\sim +5\,\text{A/m}^2$ is predicted by these two terms even in the stationary state, $\partial E_r/\partial t = 0$.

Next, the contribution of the Reynolds stress term is discussed. The turbulent Reynolds stress is defined as $\Pi_{r\theta} \equiv \langle \tilde{v}_r \tilde{v}_\theta \rangle = -k_r k_\theta S^2/2B^2$. The negative divergence of the Reynolds stress, $-r^{-1}\partial r \Pi_{r\theta}/\partial r$, represents the net
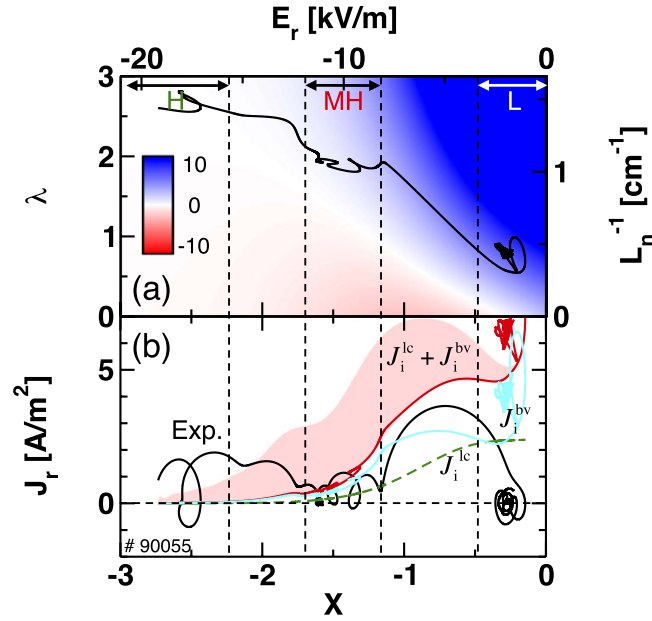
Figure 3. (**a**) Theoretical prediction of net radial current density (the sum of the loss-cone loss current J_i^{lc} and the neoclassical bulk viscosity current J_i^{bv}) as a function of normalized radial electric field X and normalized inverse density gradient length λ. The trajectory of the experimental parameters (X, λ) is overplotted. (**b**) Radial current densities (experimental observation, total theoretical prediction, and each term J_i^{lc} and J_i^{bv}) as a function of normalized radial electric field. The trajectories for J_i^{lc} and J_i^{bv} are for the case assuming $\partial T_i/\partial t = 0$.

influx of the poloidal momentum into the radius of interest, i.e., the Reynolds force. Corresponding radial current is given as

$$J_i^{\nu \nabla \nu} = -en_e \omega_{ci}^{-1} r^{-1}\frac{\partial r \Pi_{r\theta}}{\partial r},$$

(7)

where ω_{ci} is the ion gyro angular frequency. Radial profile of $\Pi_{r\theta}$ and $-r^{-1}\partial r\Pi_{r\theta}/\partial r$ in the L-mode are shown in Fig. 2(e,f). Here we assume that the poloidal wavenumber k_θ to be constant within the radial turbulence correlation length of several centimeters at the edge[14,28]. The radial current induced by the turbulent Reynolds stress is given as $J_i^{\nu \nabla \nu} \sim -0.2\,\text{A/m}^2$ at $r - a \sim -0.6\,\text{cm}$ in the L-mode, which has only a small contribution compared with the other terms. In order to alter this result, an order of magnitude change in k_θ within the turbulence correlation region is required, which is not reasonable. The large positive current of $J_i^{lc} + J_i^{bv}$ in the L-mode [Fig. 3(b)] is not compensated with the current caused by the Reynolds stress. The unimportant role of the Reynolds stress was also confirmed in the LCO in the present discharge[18]. At the plasma boundary $-r^{-1}\partial r\Pi_{r\theta}/\partial r$ and $J_i^{\nu \nabla \nu}$ have a large positive value. The boundary limits the radial propagation of the turbulence which brings a flip of the sign in the radial wavenumber and therefore the large gradient in $\Pi_{r\theta}$. The current balance in the plasma edge should also be discussed in future. In the MH-mode, the turbulent Reynolds stress and Reynolds force decay down below one half of the values in the L-mode, and almost disappear after the final MH-H transition.

Discussion and Summary

In the L-mode, the sum of the first three terms in Eq. (4), $J_i^{lc} + J_i^{bv} + J_i^{\nu \nabla \nu}$, does not agree with the experimental observation, which indicates importance of the other contributions. The most probable candidate that can achieve the ambipolar condition in the L-mode is the wave convection current term J_{e-i}^{wave}, which is related to the convective loss of the wave momentum. An intuitive model of J_{e-i}^{wave} is given in ref. 2 as

$$J_{e-i}^{wave} = -en_e D_e \rho_p^{-1}(-\lambda - X),$$

(8)

where D_e is the typical turbulent diffusivity and should be a function of E_r. In the present case J_{e-i}^{wave} leads to a negative current whose absolute value is comparable with that of J_i^{bv} when $|X| \ll 1$, i.e., in the L-mode. This can compensate the excess prediction by $J_i^{lc} + J_i^{bv}$ in the L-mode. After the L-H transition where the turbulence activity is suppressed, impact of J_{e-i}^{wave} may sharply decrease as E_r grows. This qualitatively explains the fact that the larger E_r grows, the smaller the deviation between the experiential J_r and the model prediction $J_i^{lc} + J_i^{bv}$ becomes as shown in Fig. 3(b). More detailed modeling for J_{e-i}^{wave} term is needed to improve quality of the prediction. Furthermore, this term is considered to be important not only for the prediction of the radial current but also for clarifying the thermal turbulent transport[29,30].

In summary, the following conclusions can be made. The discharge is characterized by a two-step transition, i.e., the L-meta-H (MH) transition and the MH-H transitions. Examining time derivative of Poisson's equation,

it is found that the sum of the loss-cone loss current and the neoclassical bulk viscosity current behaves similar to the experimentally observed radial current within a few factors of magnitude during the L-MH transition. The Reynolds stress term only plays a minor role. The MH-H transition cannot be explained with the present models. In the L-mode, the sum of the loss-cone loss current and the neoclassical bulk viscosity current provides an excess positive current offset, indicating importance of the other terms. The wave convection current might be a candidate to satisfy the ambipolar current condition in the L-mode, but further modeling works are needed for more quantitative conclusion.

Methods

JFT-2M. JFT-2M is a medium size tokamak with a major radius (R) of 1.3 m and an averaged minor radius (a) of 0.3 m. The present experimental conditions are as follows; the neutral beam injection (NBI) power P_{NB} of 750 kW, the toroidal magnetic field B of 1.17 or 1.28 T, the safety factor at the flux surface enclosing 95% of the total poloidal flux, q_{95}, of 2.9, the plasma current I_p of 190 kA, and the line averaged electron density $\bar{n}_e$ of $1.1 \times 10^{19}\,m^{-3}$ before the L-H transition. At the plasma edge, the ion collisionality is slightly below unity, so that the neoclassical transport is in the banana regime. An upper single-null divertor configuration is employed, where the ∇B drift of ions is directed toward the X-point. JFT-2M has been shutdown in 2004.

Heavy Ion Beam Probe (HIBP). The HIBP on JFT-2M has a primary beam energy of $W_0 = 350$ keV. The electrostatic potential ϕ and the electron density n_e can be simultaneously measured at four sample volumes (6 mm × 2 mm) on the different magnetic surfaces[31]. Radial distance between each sample volume projected in the outer midplane is ~2.5 mm. Sampling time of the system is 1 μs, so that structure and turbulence can be measured simultaneously. Precise tuning of the HIBP measurement conditions, such as the primary beam energy, the toroidal magnetic field, and the incident angle of the beam, realizes two different measurement setups: the angle between the row of the sample volumes and the normal vector of the magnetic surface is set to be either 0 or ~$\pi/3$[31]. The poloidal wavenumber of turbulence k_θ can be determined by the former setup. The radial wavenumber k_r can be deduced from the poloidal wavenumber k_θ and the wavenumber along the line of the sample volumes k_{path}, which is evaluated from the latter condition[18]. The latter condition can also be used for the radial profile measurement, assuming that the plasma parameters such as the electrostatic potential and the electron density are constant on a magnetic surface.

References

1. Wagner, F. *et al.* Regime of improved confinement and high beta in neutral-beam-heated divertor discharges of the ASDEX Tokamak. *Phys. Rev. Lett.* **49,** 1408–1412 (1982).
2. Itoh, S.-I. & Itoh, K. Model of L to H-mode transition in tokamak. *Phys. Rev. Lett.* **60,** 2276–2279 (1988).
3. Shaing, K. C. & Crume, E. C., Jr. Bifurcation theory of poloidal rotation in tokamaks: A model for L-H transition. *Phys. Rev. Lett.* **63,** 2369 (1989).
4. Kim, E. J. & Diamond, P. H. Zonal flows and transient dynamics of the LH transition. *Phys. Rev. Lett.* **90,** 185006 (2003).
5. Biglari, H., Diamond, P. H. & Terry, P. W. Influence of sheared poloidal rotation on edge turbulence. *Phys. Fluids B* **2,** 1 (1990).
6. Itoh, S.-I. & Itoh, K. Change of Transport at L- and H-Mode Transition. *J. Phys. Soc. Jpn.* **59,** 3815 (1990).
7. Groebner, R. J., Burrell, K. H. & Seraydarian, R. P. Role of edge electric field and poloidal rotation in the LH transition. *Phys. Rev. Lett.* **64,** 3015 (1990).
8. Ida, K. *et al.* Edge electric-field profiles of H-mode plasmas in the JFT-2M tokamak. *Phys. Rev. Lett.* **65,** 1364–1367 (1990).
9. Burrell, K. H. Effects of E × B velocity shear and magnetic shear on turbulence and transport in magnetic confinement devices. *Phys. Plasmas* **4,** 1499 (1997).
10. Itoh, K. & Itoh, S.-I. The role of the electric field in confinement. *Plasma Phys. Control. Fusion* **38,** 1 (1996).
11. Fujisawa, A. *et al.* Dynamic Behavior of Potential in the Plasma Core of the CHS Heliotron/Torsatron. *Phys. Rev. Lett* **79,** 1054 (1997).
12. Weynants, R., Taylor, R. *et al.* Dynamics of H-mode-like edge transitions brought about by external polarization. *Nucl. Fusion* **30,** 945 (1990).
13. Stringer, T. E. *et al.* Explanation of the L-H mode transition induced by applied voltage. *Nucl. Fusion* **33,** 1249 (1993).
14. Shesterikov, I., Xu, Y. *et al.* Experimental Evidence for the Intimate Interaction among Sheared Flows, Eddy Structures, Reynolds Stress, and Zonal Flows across a Transition to Improved Confinemen. *Phys. Rev. Lett.* **111,** 055006 (2013).
15. Kasuya, N., Itoh, K. & Takase, Y. Effect of electrode biasing on the radial electric field structure bifurcation in tokamak plasmas. *Nucl. Fusion* **43,** 244 (2003).
16. Conway, G. D. *et al.* Mean and Oscillating Plasma Flows and Turbulence Interactions across the LH Confinement Transition. *Phys. Rev. Lett.* **106,** 65001 (2011).
17. Schmitz, L. *et al.* Role of Zonal Flow Predator-Prey Oscillations in Triggering the Transition to H-Mode Confinement. *Phys. Rev. Lett.* **108,** 155002 (2012).
18. Kobayashi, T. *et al.* Spatiotemporal Structures of Edge Limit-Cycle Oscillation before L-to-H Transition in the JFT-2M Tokamak. *Phys. Rev. Lett.* **111,** 035002 (2013).
19. Rosenbluth, M. N. & Hinton, F. L. Poloidal flow driven by ion-temperature-gradient turbulence in tokamaks. *Phys. Rev. Lett.* **80,** 724–727 (1998).
20. Pütterich, T. *et al.* Evidence for Strong Inversed Shear of Toroidal Rotation at the Edge-Transport Barrier in the ASDEX Upgrade. *Phys. Rev. Lett.* **102,** 025001 (2009).
21. Kamiya, K. *et al.* Boundary condition for toroidal plasma flow imposed at the separatrix in high confinement JT-60U plasmas with edge localized modes and the physics process in pedestal structure formation. *Phys. Plasmas* **21,** 122517 (2014).
22. Ido, T. *et al.* Observation of the Fast Potential Change at L-H Transition by a Heavy-Ion-Beam Probe on JFT-2M. *Phys. Rev. Lett.* **88,** 055006 (2002).
23. Kobayashi, T. *et al.* Edge plasma dynamics during L-H transition in the JFT-2M tokamak. *Nucl. Fusion* **55,** 063009 (2015).
24. Diamond, P. H. & Kim, Y.-B. Theory of mean poloidal flow generation by turbulence. *Phys. Fluids B* **3,** 1626 (1991).
25. Itoh, K. & Itoh, S.-I. Influence of the wall material on the H-mode performance. *Plasma Phys. Control. Fusion* **37,** 491 (1995).
26. Fried, B. D. & Conte, S. D. *The Plasma Dispersion Function* (New York: Academic, 1961).
27. Viezzer, E. *et al.* Evidence for the neoclassical nature of the radial electric field in the edge transport barrier of ASDEX Upgrade. *Nucl. Fusion* **54,** 012003 (2013).
28. Ido, T. *et al.* Geodesic-acoustic-mode in JFT-2M tokamak plasmas. *Plasma Phys. Control. Fusion* **48,** S41 (2006).
29. Ritz, C. P. *et al.* Fluctuation-Induced Energy Flux in the Tokamak Edge. *J. Nucl. Mater.* **145–147,** 241 (1987).

30. Wootton, A. J. *et al.* Fluctuations and anomalous transport in tokamaks. *Phys. Fluids B* **2,** 2879 (1990).
31. Ido, T. *et al.* Observation of the interaction between the geodesic acoustic mode and ambient fluctuation in the JFT-2M tokamak. *Nucl. Fusion* **46,** 512 (2006).

Acknowledgements

Author Contributions

T.I., K.K., Y.M. and K.H. conducted the experiments. T.I. and K.H. provided the HIBP data. T.K. analyzed the data. K. Itoh and S.-I.I. provided the theoretical models. T.K., K. Itoh, T.I., K.K., S.-I.I., Y.N., A.F., S.I. and K. Ida discussed the model validation. T.K. and K. Itoh wrote the main manuscript text and all authors reviewed the manuscript.

Additional Information